OXFORD

Research Article

Notch4 participates in mesenchymal stem cell-induced differentiation in 3D-printed matrix and is implicated in eccrine sweat gland morphogenesis

Yuzhen Wang [iD] [1,2,†], **Fanliang Zhang** [1,†], **Bin Yao** [3,†], **Linhao Hou** [4], **Zhao Li** [1], **Wei Song** [1], **Yi Kong** [1], **Yaxin Tan** [5], **Xiaobing Fu** [1,*] and **Sha Huang** [iD] [1,*]

[1] Research Center for Tissue Repair and Regeneration affiliated to the Medical Innovation Research Department, Chinese PLA General Hospital, 28 Fu Xing Road, Beijing, 100853, P. R. China, [2] Department of Burn and Plastic Surgery, Air Force Hospital of Chinese PLA Central Theater Command, 589 Yunzhong Road, Pingcheng District, Datong, Shanxi, 037006, P. R. China, [3] Academy of Medical Engineering and Translational Medicine, Tianjin University, 92 Weijin Road, Nankai District, Tianjin, 300072, P. R. China, [4] Department of Orthopedics, the Fourth Affiliated Hospital of China Medical University, 4 Chongshan East Road, Shenyang, 110032, P. R. China and [5] College of Graduate, Tianjin Medical University, 22 Qi Xiang Tai Road, Heping District, Tianjin, 300070, P.R. China

*Correspondence. Xiaobing Fu, Email: fuxiaobing@vip.sina.com; Sha Huang, Email: stellarahuang@sina.com

[†] These authors contributed equally to this work.

Abstract

Background: Eccrine sweat gland (SG) plays a crucial role in thermoregulation but exhibits very limited regenerative potential. Although SG lineage-restricted niches dominate SG morphogenesis and benefit SG regeneration, rebuilding niches *in vivo* is challenging for stem cell therapeutic applications. Hence, we attempted to screen and tune the critical niche-responding genes that dually respond to both biochemical and structural cues, which might be a promising strategy for SG regeneration.

Methods: An artificial SG lineage-restricted niche consisting of mouse plantar dermis homogenates (i.e. biochemical cues) and 3D architecture (i.e. structural cues) was built *in vitro* by using an extrusion-based 3D bioprinting approach. Mouse bone marrow-derived mesenchymal stem cells (MSCs) were then differentiated into the induced SG cells in the artificial SG lineage-restricted niche. To decouple biochemical cues from structural cues, the transcriptional changes aroused by pure biochemical cues, pure structural cues and synergistic effects of both cues were analyzed pairwise, respectively. Notably, only niche-dual-responding genes that are differentially expressed in response to both biochemical and structural cues and participate in switching MSC fates towards SG lineage were screened out. Validations *in vitro* and *in vivo* were respectively conducted by inhibiting or activating the candidate niche-dual-responding gene(s) to explore the consequent effects on SG differentiation.

Results: Notch4 is one of the niche-dual-responding genes that enhanced MSC stemness and promoted SG differentiation in 3D-printed matrix *in vitro*. Furthermore, inhibiting Notch4 specifically reduced keratin 19-positive epidermal stem cells and keratin 14-positive SG progenitor cells, thus further delaying embryonic SG morphogenesis *in vivo*.

Conclusions: Notch4 not only participates in mouse MSC-induced SG differentiation *in vitro* but is also implicated in mouse eccrine SG morphogenesis *in vivo*.

Graphical Abstract
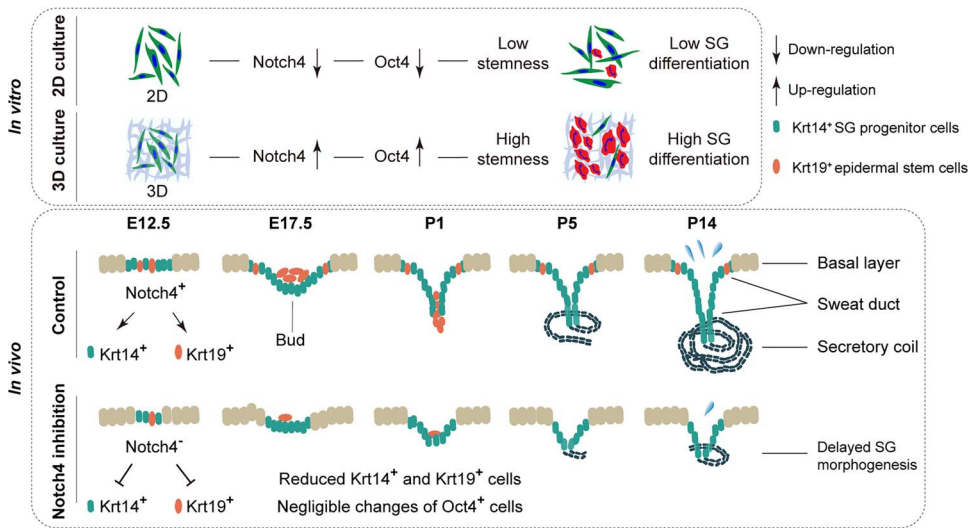
Key words: Mesenchymal stem cells, Notch, Stem cell–microenvironment interactions, Stem cell plasticity, Differentiation, Sweat gland, 3D bioprinting, Regeneration

Highlights

- 3D-cultured MSCs exhibit higher SG differentiation efficiency than 2D-cultured MSCs.
- 3D-printed architectures enhanced Oct4-related MSC stemness by regulating Notch4.
- Notch4 participates in mesenchymal stem cell-induced SG differentiation in 3D-printed matrix *in vitro*.
- Inhibiting Notch4 delayed SG morphogenesis by reducing SG progenitor cells *in vivo*.

Background

Eccrine sweat glands (SGs) consist of ducts and secretory coils and play crucial roles in thermoregulation and metabolism, serving as the most abundant glandular structures with a density of 200–700/cm² of human skin surface [1]. SGs are also vulnerable to injuries and exhibit very limited regenerative potential. Survivors who have suffered from abundant SG injuries caused by large-area burns are subject to hyperthermia, heat stroke or even death in hot environments or during long-term exercise [2]. However, despite recent progress involving SG morphogenesis mechanisms [3] and stem cell-based regenerative therapies [4], SG regeneration with anatomical structures and restored biofunction (i.e. secreting sweat) is far from clinical or translational application.

In mice, embryonic SGs originate from the basal layer of epidermis and emerge as the sweat buds, a group of branching epitheliums that mainly consist of keratin (Krt) 19-positive epidermal stem cells and Krt14-positive SG progenitor cells at about embryonic day (E) 17.5 [5]. SG ducts and secretory coils respectively emerge at about postpartum day (P) 1 and P5, and anatomical SGs with secreting bio-functions

mature until about P14 [6]. Biologically, Krt18 and Krt14 serve as phenotypic biomarkers and are distributed in SG secretory ducts or myoepithelium, and ATPase Na⁺/K⁺ transporting subunit alpha 1 (ATP1a1) and aquaporin 5 (Aqp5) serve as functional biomarkers and are associated with transporting ions or water during sweating processes.

A niche is the lineage-restricted microenvironment that both anatomically and functionally maintains stem cell self-renewal [7] and directs stem cell fate towards a defined lineage [8]. Generally, niches interact with stem cells through biochemical cues (i.e. bioactive proteins, growth factors, cytokines, ions, signaling pathways, extracellular matrix, etc.) [9] and structural cues (i.e. 3D architecture, pore sizes, topology, matrix stiffness, applied forces, etc.) [10]. Despite the origins of stem cells [11], a niche sometimes gets the ascendancy in directing their lineage [12]. Reportedly, it has been shown with skin organoids that only in a 3D culture environment *in vitro* together with defined biochemical factors can stem cells mimic *in vivo* SG morphogenesis processes [13–15], which indicates that both biochemical and structural cues are indispensable for bio-functional SG lineage-restricted niches. Recent progress highlighted the

crucial roles of niches in regulating embryonic SG morphogenesis [16], and rebuilding SG lineage-restricted niches with defined biochemical and structural cues successfully switched the fates of stem cells towards SG lineages in mice [17–19].

Notably, the mouse plantar dermis (PD) is believed to contain SG lineage-restricted niches [20] because mouse SGs are restrictedly distributed in foot pads [5]. Very recently, we rebuilt artificial SG niches consisting of PD homogenates (i.e. biochemical cues) and 3D-printed architecture (i.e. structural cues) and then directed mouse bone marrow-derived mesenchymal stem cells (MSCs) towards SG lineages and facilitated SG regeneration in mice [21]. However, rebuilding SG lineage-restricted niches *in vivo* is an insurmountable challenge because it is difficult to synergistically orchestrate these biochemical and structural cues in ever-changing wound environments. Moreover, the PD homogenates that are harvested from mouse foot pads are difficult to use in stem cell-based therapeutic applications especially for human beings. With regard to translational medicine, we tend to explore how stem cells interact with SG lineage-restricted niches by filtering the candidate genes that dually respond to both biochemical and structural cues of niches. Tuning these critical niche-dual-responding genes might represent a promising strategy for progressing SG regenerative therapies to the clinic.

Here, we rebuilt artificial SG lineage-restricted niches and then directed mouse MSCs into the induced SG cells (iSGs) in a PD-containing 3D-printed matrix. To decouple biochemical cues from structural cues, we pairwise compared the transcriptional changes aroused by pure biochemical cues, pure structural cues, and synergistic effects of both cues, respectively. Notably, only niche-dual-responding genes that respond to both biochemical and structural cues and are crucial for SG differentiation were screened out using RNA-sequencing and gene ontology (GO) enrichment analyses. Validations were conducted by inhibiting or activating the candidate niche-dual-responding gene(s) both *in vitro* and *in vivo*, respectively. Our study attempts to provide new strategies targeting niche-dual-responding genes for progressing stem cell-based SG regeneration therapeutics to the clinic.

Methods

Mice

All animal experiments were performed in accordance with EU Directive 2010/63/EU on the protection of animals used for scientific purposes. C57BL/6 mice used in this study were purchased from Sibeifu Biotechnology Co., Ltd (Beijing, China). All mice were caged with food and tap water *ad libitum* in a specific-pathogen-free facility. In order to precisely mark the embryonic day ages, male and female mice were caged together for one night and were separated the next morning. If the female mice were later found to be pregnant, this time point was marked as E 0.5. Pregnant female mice were caged separately without any unnecessary treatments. The first author was aware of the group allocation at the different stages of the experiments, and mice were randomly selected by another independent researcher for subsequent studies. The Institutional Animal Care and USE Committee of Chinese PLA General Hospital (Beijing, China) approved the animal experiments (approval number SCXK(BJ)2019–0001) and supervised the animal welfares of this study.

Isolating MSCs and preparing PD homogenates

MSCs were isolated and cultured as previously reported [17]. The tibias and femurs were harvested from legs of newborn mice (P1) after removing the skin, fascia and muscles, and then were cut into pieces and incubated with type I collagenase solution (containing 0.25% type I collagenase and 20% fetal bovine serum) with occasional shaking at 37°C for 45 min. After centrifugation at 350 g for 10 min, the primary MSCs were harvested and incubated with complete MesenCult™ medium (Mouse, STEMCELL, Canada). MSCs with 3–4 cell passages were used for subsequent experiments.

PD homogenates were prepared based on our previous work [21]. Briefly, dermal tissues from foot pads of newborn mice (P1) were separated after being immersed in 0.2% (w/v) Dispase II (neutral protease, grade II; Roche, Germany) solution, and were then triturated and homogenized to a final concentration of 25% (w/v). After centrifugation at 10,000 g for 20 min at 4°C, the supernatants, i.e. the PD homogenates, were filtered through a 0.22 μm filter. The protein concentrations of the PD homogenates were tested and uniformized using a BCA Protein Assay Kit (CW00145, Cwbiotech, China).

Inducing MSCs differentiate into SG lineages with formulated bioinks and 3D bioprinting

MSCs and PD homogenates were involved in bioinks and were printed into 3D constructs, and were then induced into SG lineages and designated as the '3D iSG' group [17]. Briefly, bioinks were formulated with 3% (w/v) type B gelatin (Sigma-Aldrich, USA) and 1% (w/v) sodium alginate (Sigma-Aldrich, USA). After being sterilized by a modified pasteurization (i.e. 30 min at 70°C a total of three times with intervals of 10 min at 4°C), every 10 ml of alginate-gelatin bioink was loaded with 1×10^7 MSC suspension and 1 ml of PD homogenate. 3D constructs were printed layer-by-layer onto a 2D platform using an extrusion-based 3D bioprinter (Bio-Architect PRO, Regenovo, China) with 280 μm-inner-diameter nozzles under a pressure of 0.1–0.4 MPa and a flow rate of 10–15 mm/s. Pre-cooled 2.5% (w/v) calcium chloride solutions were used to crosslink the 3D-printed constructs for 10 min. After crosslinking, the 3D-printed constructs were incubated with MSC medium (mouse complete MesenCult™ medium, STEMCELL, Canada) for 3 days, and then incubated with SG medium and additional PD homogenate for another 4 days (Figure 1a). Specifically, the SG medium contains 50% F12 (STEMCELL, Canada), 50% DMEM (STEMCELL, Canada) basal culture medium, and a list of supplements, including liothyronine sodium (2 ng/ml, Gibco), hydrocortisone succinate (0.4 mg/ml, Gibco), epidermal growth factor (10 ng/ml, Peprotech, Rocky Hill, NJ, USA), 1% (v/v) insulin-transferrin-selenium (Gibco), 5% (v/v) fetal calf serum (Gibco) and 1% (v/v) penicillin–streptomycin solutions.
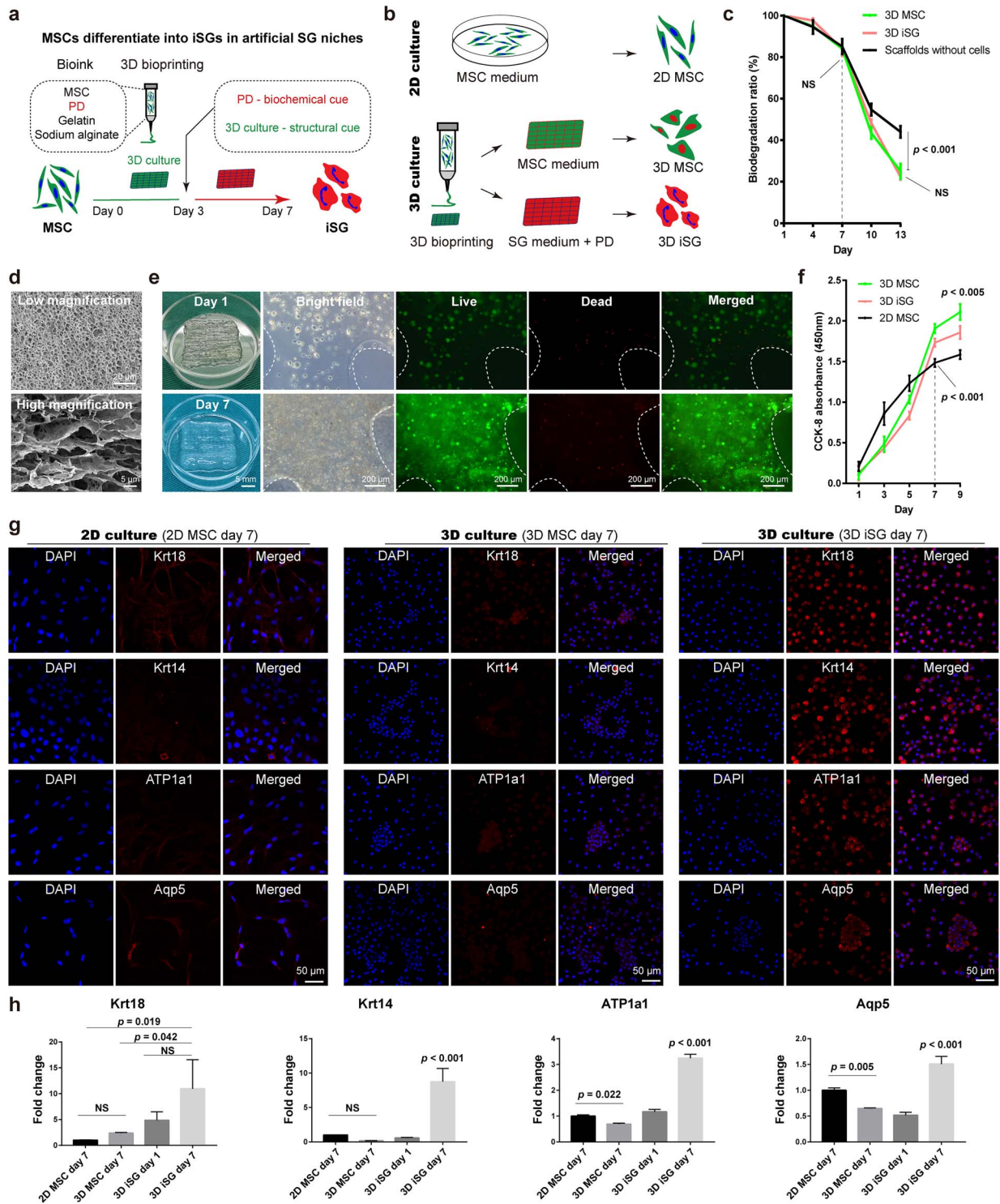
Figure 1. MSCs differentiate into iSGs *in vitro* due to biochemical and structural cues. Schematic drawings illustrate the MSC-derived iSGs in artificial SG niches (**a**) and three groups of cell samples for RNA sequencing (**b**). (**c**) Biodegradation ratio (%) of 3D MSC group, 3D iSG group, and pure scaffolds without cells; n = 4. (**d**) Scanning electron microscopy images at the low and high magnification of the 3D-printed constructs at day 1. (**e**) Macrograph pictures and bright field images indicate good printability, and live/dead test indicates good cell biocompatibility. Dotted curves indicate the pore edges within 3D-printed constructs. (**f**) Cell counting kit-8 proliferation assays of 2D MSC, 3D MSC and 3D iSG groups; n = 4. MSC-derived iSGs were characterized by four SG biomarkers (Krt18, Krt14, ATP1a1 and Aqp5) using immuno-fluorescence staining (**g**) and RT-qPCR (**h**); *n* = 3. Scale bar (d): 20 μm, 5 μm; (e): 5 mm, 200 μm; (g): 50 μm. *ATP1a1* ATPase Na+/K+ transporting subunit alpha 1, *Aqp5* aquaporin 5, *iSG* induced sweat gland, *Krt* keratin, *MSCs* mesenchymal stem cells, *NS* no significant difference, *RT-qPCR* real-time quantitative polymerase chain reaction, *SG* sweat gland

In addition, the '2D MSC' group (i.e. conventionally cultured MSCs on Petri dishes using MSC medium) and '3D MSC' group (i.e. 3D cultured MSCs in 3D-printed constructs without PD homogenates using MSC medium) were employed as control groups (Figure 1b).

Biodegradation ratio

The biodegradation properties were detected between 3D MSC groups and 3D iSG groups that were seeded with equal number of cells at days 1, 4, 7, 10 and 13, and bio-printed scaffolds without cells were employed as control groups. Briefly, these samples were first incubation at 37°C with cell culture medium, and were then rinsed with 0.01 M phosphate-buffered saline (PBS) followed with drying overnight in a 70°C drying oven to remove as much water as possible. As the newly printed constructs can absorb water due to swelling properties, the mean dry weights of each group at day 1 were regarded as the initial weights (100%), and the decreased dry weights of each group were measured at each time point. The ratios of the decreased weights to the initial weights were calculated as the biodegradation ratio (%). Each group at each time point included four independent samples ($n = 4$).

Scanning electron microscopy

The surface structures and inner microstructures of the 3D-printed constructs were observed by means of scanning electron microscopy at day 1. Briefly, the samples were cross-sectioned with a sharp knife, and were fixed in 0.5% glutaraldehyde for 24 h at room temperature followed by dehydration in a graded ethanol series, and then Au sputter-coated for 60 s under high-vacuum conditions at an accelerating voltage of 10.0 kV. The images of the cross-sections were captured to characterize the surface structures and inner microstructures.

Cell counting kit-8 proliferation assays

The cell numbers in 3D MSC groups and 3D iSG groups were detected using cell counting kit-8 proliferation assays at days 1, 3, 5, 7 and 9, with the 2D MSC groups that were seeded with equal number of cells as control groups. Briefly, samples were removed into a new 96-well plate with 100 μl of culture medium in each well. After incubation for 2 h, 10 μl of cell counting kit-8 solution (Dojindo, Kyushu, Japan) was added into each well. After incubation at 37°C for 3 h, the mean optical density values of the culture medium were quantitated at a wavelength of 450 nm using an enzyme-linked immunosorbent assay reader (Thermo Varioskan Flash, USA). Each group at each time point included four independent samples ($n = 4$).

2D and 3D cell morphology and histological study of SG morphogenesis

The cell viability in 3D constructs was tested by a Live/Dead® Viability/Cytotoxicity Kit (Invitrogen, USA) after printing at days 1 and 7. Cell morphology on 2D-cultured Petri dishes or in 3D-printed constructs was observed and recorded using a phase-contrast microscope (Leica DMI4000B, Germany).

To observe 3D-cultured cellular morphology, cells that were embedded in 3D matrix were isolated by dissolving the 3D-printed constructs using a mixture of sodium chloride (150 mM), ethylene diamine tetraacetic acid disodium salt (20 mM) and sodium citrate (55 mM). The suspensions of 3D-cultured cells isolated from 3D-printed constructs were successively fixed, centrifuged, resuspended and then transferred onto adhesive slides. After being dried at 60°C for 30 min, the isolated cells that were originally cultured in 3D constructs were coated onto the surface of slides for conventional immunofluorescence staining. Cells from the 3D MSC and 3D iSG groups were isolated at day 7 and immunofluorescence stained with SG biomarkers respectively, with 2D MSC groups as control groups.

To observe SG morphogenesis, E12.5, E17.5, P1, P5 and P14 aged embryos or mice were sacrificed, and the foot pads were harvested and fixed in 4% paraformaldehyde solution for 2 days. Then these foot pads were immersed in decalcifying mixed solutions (Solarbio, G2470) containing ethylene diamine tetraacetic acids, formic acid, formaldehyde, etc. for 2 days in order to remove calcium in bones, and were then embedded in paraffin and sectioned 6-μm thick using a cryotome (Leica, CM1950, Germany) followed by histological studies.

As 3D-cultured cells are embedded within alginate-gelatin bioinks and thus it is difficult to conduct immunofluorescence staining with routinely conventional protocols, the crosslinked bioinks have to be dissolved so that the cells can be re-collected by centrifuge and re-loaded on the surfaces of object slides for conventional immunofluorescence staining.

For immuno-fluorescence analysis, the slides underwent antigen retrieval and infiltration, and were then blocked to avoid non-specific antigen reactions. For detecting SG biomarkers, the slides were incubated with anti-Krt18 mouse monoclonal antibody (1 : 250, ab668, Abcam), anti-Krt14 mouse monoclonal antibody (1 : 300, ab7800, Abcam), anti-ATP1a1 mouse monoclonal antibody (1 : 300, ab7671, Abcam) and anti-Aqp5 rabbit polyclonal antibody (1 : 500, ab78486, Abcam). For detecting the relationships between Notch4 and Oct4, the slides were incubated with anti-Notch4 mouse monoclonal antibody (1 : 100, sc-393 893, Santa Cruz) and anti-Oct4 rabbit polyclonal antibody (1 : 250, ab18976, Abcam). For detecting the effects of inhibiting or activating Notch signals on SG differentiation *in vitro*, the slides were incubated with anti-Notch4 rabbit monoclonal antibody (1 : 250, ab184742, Abcam) and anti-Krt18 mouse monoclonal antibody (1 : 250, ab668, Abcam). For detecting the effects of inhibiting Notch4 on SG morphogenesis *in vivo*, the slides were incubated with anti-Notch4 rabbit monoclonal antibody (1 : 250, ab184742, Abcam) and anti-Krt14 mouse monoclonal antibody (1 : 300, ab7800, Abcam). All these first antibodies were incubated overnight at 4°C. After rinsing,

the slides were incubated with CoraLite488-conjugated goat-anti-mouse (1 : 250, SA00013–1) or goat-anti-rabbit (1 : 250, SA00013–2), or CoraLite594-conjugated goat-anti-mouse (1 : 250, SA00013–3) or goat-anti-rabbit (1 : 250, SA00013–4) secondary antibody for 2 h and subsequent staining of cell nuclei with DAPI Fluoromount-G® (0100–20, Southern Biotech). A laser scanning confocal microscope (Leica, SP8 FALCON, Germany) was used to capture fluorescence images.

For immuno-histochemical analysis, anti-Notch4 rabbit monoclonal antibody (1 : 500, ab184742, Abcam), anti-Oct4 rabbit polyclonal antibody (1 : 250, ab18976, Abcam) and anti-Krt19 rabbit monoclonal antibody (1 : 250, ab52625, Abcam) were incubated overnight, and after rinsing off primary antibodies, were incubated with biotinylated goat-anti-rabbit immunoglobulins as secondary antibody, with subsequent counterstaining with Mayer's hematoxylin as well as dehydration and addition of coverslips.

RNA sequencing and gene ontology analysis

At day 7, the total RNA of '2D MSC', '3D MSC' and '3D iSG' groups (Figure 1b, each with three independent biological replicates) was extracted using TRIzol reagents (Invitrogen, USA), respectively. RNA sequencing analysis was performed with HiSeq 2500 (Illumina). Gene expression with |log$_2$ fold change| > 1.0, mean log intensity >2.0 and false discovery rate < 0.05 were considered to be significant.

Gene ontology (GO) enrichment analysis was carried out using the Metascape online tool (https://metascape.org), which performs hierarchical clustering of the enriched terms based on inputted genes and then outputs an enrichment result that indicates the most significant GO term within a cluster. Overlapping the genes involved in related GO terms represents a well-used approach for filtering candidate genes [20].

Real-time quantitative polymerase chain reaction

After extracting total RNA using TRIzol reagents (Invitrogen, USA) and detecting RNA concentrations using a Nano Photometer (Implen GmbH, P-330-31, Germany), Prime-Script RT reagent Kit with gDNA Eraser (Takara, China) was used for reverse transcription. Gene expression was quantitatively analyzed by using TB Green Premix Ex Taq II (Takara, China) on a QuantStudio 5 system (Applied Biosystems, USA). The $2^{-\triangle\triangle CT}$ methods were used and gene expression was normalized to glyceraldehyde-3-phosphate dehydrogenase (GAPDH). The primers of targeted genes are shown in Table 1.

Western blotting

Cells were lysed on ice and total protein was extracted using pre-cooled RIPA lysis buffer (P0013B, Beyotime) with protease inhibitors (Roche), followed by measurement of protein concentrations by BCA protein assay kit (CW00145, Cwbiotech, China). After being centrifuged, quantified and denatured, 80 μg protein samples were separated by 12% sodium dodecyl sulfate polyacrylamide gel electrophoresis and were then transferred onto methanol-activated polyvinylidene difluoride membranes (GE Healthcare, USA). Bovine serum albumin solutions (5%) were used to block non-specific antigens for 1.5 h. The membranes were probed with anti-Notch4 rabbit monoclonal antibody (1 : 500, ab184742, Abcam), anti-Oct4 rabbit monoclonal antibody (1 : 500, ab18976, Abcam), anti-Krt18 mouse monoclonal antibody (1 : 500, ab668, Abcam) or anti-GAPDH mouse monoclonal antibody (1 : 1000, 60 004–1-Ig, Proteintech). Protein bands were visualized using a UVITEC Alliance MINI HD9 instrument (UVITEC, UK) with an enhanced chemiluminescence detection system.

Activating or inhibiting of Notch signaling pathways

The Notch signaling pathway was activated by valproic acid (VPA) [22], a small molecular branched-chain fatty acid extracted from *Valeriana officinalis* with the ability to specifically bind to the catalytic center of histone deacetylase [23]. VPA powder (ab120745, Abcam) was dissolved in 0.01 M PBS to 100 mM as stock solution and then added into the cell culture medium to a final concentration of 1 mM [24]. The control group received an equal volume of PBS.

The Notch signaling pathway was inhibited by *N*-[*N*-(3,5-difluorophenacetyl-L-alanyl)]-(*S*)-phenylglycine *t*-butyl ester (DAPT), a small molecular gamma-secretase inhibitor that prevents cleavage of Notch receptors, resulting in decreased Notch intracellular domain [25]. To inhibit Notch signaling in cultured cells, DAPT powder (ab120633, Abcam) was dissolved in dimethyl sulfoxide (DMSO) to 100 mM as stock solution and then were added into the cell culture medium to a final concentration of 20 μM [26].

To inhibit Notch signaling in mice, DAPT powder was dissolved in 0.01 M PBS containing 5% DMSO to a final concentration of 1 mg/ml and then 1 mg/kg per mouse was injected intraperitoneally [27]. To avoid corrosive injuries directly cause by DMSO to mouse embryos, DAPT solutions were injected intraperitoneally into separately-caged males (9) and females (12) that were not yet pregnant once daily for 5 days, and then these DAPT-treated male and female mice were caged together. E12.5, E17.5, P1, P5 and P14 aged embryos or mice were sacrificed to check the process of SG morphogenesis (Figure 5a). Furthermore, to specifically inhibit Notch4 receptors without disturbing other Notch signaling-related molecules, anti-Notch4 monoclonal antibody (5 mg/kg per mouse, sc-393 893, Santa Cruz) was intraperitoneally injected into two pregnant mice once daily for 2 days [28]. E17.5 and P14 aged embryos or mice were sacrificed to check the process of SG morphogenesis (Figure 6a).

Statistical analysis

Statistical analysis was performed using the Statistical Package for the Social Sciences software 13.0 (SPSS Inc., Chicago, IL, USA). The normality of all the quantitative data was tested

Table 1. Primers of genes for real-time quantitative polymerase chain reaction

Categories	Primers	Sequences (5′ to 3′)	
Sweat gland marker genes	Krt18	Forward	TCAAGATCATCGAAGACCTGAGG
		Reverse	GCGCATGGCTAGTTCTGTC
	Krt14	Forward	AGCGGCAAGAGTGAGATTTCT
		Reverse	CCTCCAGGTTATTCTCCAGGG
	ATP1a1	Forward	GGGGTTGGACGAGACAAGTAT
		Reverse	CGGCTCAAATCTGTTCCGTAT
	Aqp5	Forward	CGGCTCAAATCTGTTCCGTAT
		Reverse	GCCAGAGTAATGGCCGGAT
Notch receptor genes	Notch1	Forward	GATGGCCTCAATGGGTACAAG
		Reverse	TCGTTGTTGTTGATGTCACAGT
	Notch2	Forward	ATGTGGACGAGTGTCTGTTGC
		Reverse	GGAAGCATAGGCACAGTCATC
	Notch3	Forward	TGCCAGAGTTCAGTGGTGG
		Reverse	CACAGGCAAATCGGCCATC
	Notch4	Forward	CTCTTGCCACTCAATTTCCCT
		Reverse	TTGCAGAGTTGGGTATCCCTG
Stemness marker genes	Oct4	Forward	GGCTTCAGACTTCGCCTCC
		Reverse	AACCTGAGGTCCACAGTATGC
	Nanog	Forward	TCTTCCTGGTCCCCACAGTTT
		Reverse	GCAAGAATAGTTCTCGGGATGAA
	Sox2	Forward	GCGGAGTGGAAACTTTTGTCC
		Reverse	CGGGAAGCGTGTACTTATCCTT
Reference gene	GAPDH	Forward	AGGTCGGTGTGAACGGATTTG
		Reverse	TGTAGACCATGTAGTTGAGGTCA

with the criterion of $p > 0.05$ as normal distribution. Data with normal distribution are presented as mean ± standard deviation, and one-way analysis of variance with a *post hoc* Bonferroni's test was used for multi-group comparisons. Data with non-normal distribution are presented as median (interquartile spacing), and the Kruskal–Wallis test was used for the difference comparison between groups. Results were deemed as statistically different if $p < 0.05$. Notably, the quantitative data from the same group at different time points were treated as independent samples in order to ensure only one single contributing factor in statistical tests.

Results

MSCs differentiate into iSGs *in vitro* due to biochemical and structural cues

As noted above, MSCs differentiated into iSGs in 3D-printed matrix (Figure 1a), and '2D MSC', '3D MSC' and '3D iSG' groups each with three independent biological replicates were employed for RNA sequencing analysis (Figure 1b). Biodegradation ratio (%) tests showed that no significant difference was detected at day 7 among all groups, and '3D MSC' and '3D iSG' groups showed greater biodegradation ratios than printed scaffolds without cells at day 13 ($p < 0.001$), but still no significant difference was detected between '3D MSC' and '3D iSG' groups (Figure 1c). Biodegradation tests indicated that bio-printed structures were stable for '3D MSC' and '3D iSG' groups during MSC committing to SG lineages during culturing periods.

Representative scanning electron microscopy cross-section images at both low and high magnification showed uniform porous inner-microstructures after printing at day 1 (Figure 1d). Representative macrograph pictures showed that the 3D-printed constructs exhibited stable 3D architecture at days 1 and 7, and bright field images under the phase-contrast microscope showed precisely controlled deposition of bioink filaments and clear pore edges at day 7 (the dotted curves indicate pore edges, Figure 1e). At day 1, there were more live cells (green color) in 3D constructs than dead cells (red color), indicating that cells survived well during extrusion-printing and ionic-cross-linking processes. At day 7, both proliferation and migration of cells were observed, resulting in a uniform distribution of embedded live cells and only negligible cell death throughout the 3D matrix (Figure 1e). Cell counting kit-8 proliferation assays showed that cell numbers in '2D MSC' groups are higher than in '3D MSC' and '3D iSG' groups from day 1 to day 5, but cell proliferation rates in '2D MSC' groups gradually slowed down because cell overgrowth led to limited immigration space and cell proliferation was inhibited by cell–cell contacts in 2D culture conditions (Figure 1f). Cell numbers in '2D MSC' groups became lower than those in '3D MSC' and '3D iSG' groups at day 7 ($p < 0.001$) and day 9 ($p < 0.005$) probably because 3D culture conditions provided more space for cell immigration (Figure 1f). Moreover, cell numbers in '3D iSG' groups are lower than those in '3D MSC' groups probably because the fate-switching to SG lineages slowed down the cell proliferation rates of MSCs (Figure 1f).

After culturing for 7 days, MSC-derived iSGs were respectively characterized by immuno-fluorescence staining (Figure 1g) and real-time quantitative polymerase chain reaction (RT-qPCR) (Figure 1h) by detecting four SG biomarkers, i.e. Krt18, Krt14, ATP1a1 and Aqp5. At day 7, the '3D iSG' group expressed stronger fluorescence intensities of Krt18, Krt14, ATP1a1 and Aqp5, while only negligible SG biomarkers were detected in the '2D MSC' group, which implied a switched cell fate from MSCs toward SG lineages (Figure 1g). At gene transcriptional level, the '3D iSG' group at day 7 expressed significantly higher gene levels of Krt14 ($p < 0.001$), ATP1a1 ($p < 0.001$) and Aqp5 ($p < 0.001$) compared with any other group. Krt18 gene expression at day 7 in the '3D iSG' group was significantly higher than in the '2D MSC' group ($p = 0.019$) and '3D MSC' group ($p = 0.042$). In addition, the gene expression of ATP1a1 ($p = 0.022$) and Aqp5 ($p = 0.005$) in the '3D MSC' group was significantly decreased compared with the '2D MSC' group at day 7 (Figure 1h).

Decoupling biochemical cues from structural cues by pairwise comparisons

In this artificially SG lineage-restricted niche, the 3D-printed architectures serve as structural cues, and PD homogenates, which theoretically contain all soluble proteins in the dermal extracellular matrix of mouse foot pads, serve as biochemical cues. To decouple PD-homogenate-endowed biochemical cues from 3D-culturing-endowed structural cues, pairwise comparisons were used to analyze RNA sequencing data. Briefly, '3D MSC *vs* 2D MSC' represents the transcriptional changes caused by pure 3D-culturing-endowed structural cues because they shared the same biochemical media but were cultured under distinctly different architectural conditions, i.e. 3D and 2D culturing environments (Figure 2a). '3D iSG *vs* 3D MSC' represents the transcriptional changes caused by pure PD-homogenate-endowed biochemical cues because both of them are cultured in similar 3D-printed matrix, but PD homogenates were only added to the '3D iSG' group (Figure 2c). By parity of reasoning, '3D iSG *vs* 2D MSC' represents the transcriptional changes caused by synergistic effects of both structural and biochemical cues (Figure 2b).

Firstly, '3D MSC *vs* 2D MSC' totally sequenced 19,420 genes. Among these genes, 12.7% were up-regulated and 15.4% were down-regulated with |$\log_2$-fold change| > 1.0, and 4.5% of genes were up-regulated and 5.3% of genes were down-regulated with |$\log_2$ fold change| > 1.5 (Figure 2a). Secondly, '3D iSG *vs* 2D MSC' totally sequenced 19,447 genes. Among these genes, 12.6% were up-regulated and 15.7% were down-regulated with |$\log_2$-fold change| > 1.0, and 4.1% of genes were up-regulated and 7.0% genes were down-regulated with |$\log_2$-fold change| > 1.5 (Figure 2b). Thirdly, '3D iSG *vs* 3D MSC' totally sequenced 19,096 genes. Among these genes, 6.8% were up-regulated and 6.7% were down-regulated with |$\log_2$-fold change| > 1.0, and 0.3% of genes were up-regulated and 0.9% of genes were down-regulated

with |$\log_2$-fold change| > 1.5 (Figure 2c). Notably, only |$\log_2$-fold change| > 1.5 genes were regarded as promising candidates for filtering wanted genes in the subsequent study.
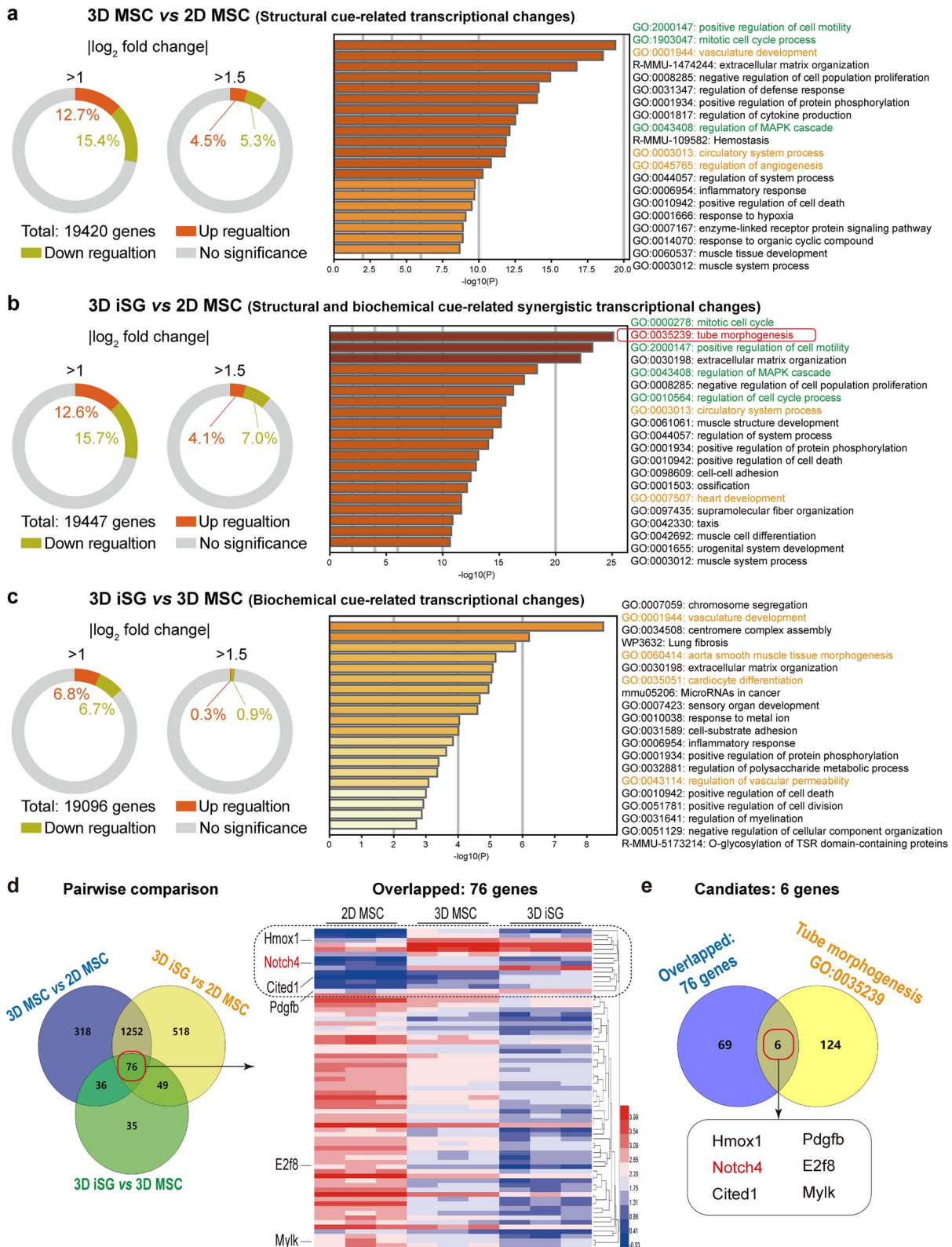
Notch4 is one of the niche-dual-responding genes and is related to MSC stemness in 3D matrix *in vitro*

Intriguingly, the cell stemness-related GO terms, such as 'positive regulation of cell motility', 'mitotic cell cycle process', 'regulation of mitogen-activated protein kinase cascade' (green font, Figure 2a, b), were enriched for '3D MSC *vs* 2D MSC' and '3D iSG *vs* 2D MSC'. However, these cell stemness-related GO terms were not enriched for '3D iSG *vs* 3D MSC' (Figure 2c). On the other hand, the angiogenesis-related GO terms, such as 'vasculature development', 'circulatory system process', 'regulation of angiogenesis', 'heart development', 'aorta smooth muscle tissue morphogenesis' (yellow font, Figure 2a–c), were enriched for all groups of pairwise comparisons. In particular, 'GO:0035239 tube morphogenesis' (red font, Figure 2b) terms are closely associated with SG morphogenesis processes.

The overlapping of up- and down- regulated genes based on pairwise comparisons totally filtered out 76 genes (Figure 2d), which are significantly changed (|$\log_2$-fold change| > 1.5) and dually respond to both structural and biochemical cues. The heat map shows that the 76 genes exhibited distinct profiles among '2D MSC', '3D MSC' and '3D iSG' groups (Figure 2d). Notably, the dotted box indicates a cluster of structural cue-responsive genes that are activated in 3D architectures (Figure 2d). To find promising gene candidates, an intersection of the differentially expressed 76 genes with 'GO:0035239 tube morphogenesis'-enriched genes was performed resulting in six overlapping genes, i.e. Hmox1, Notch4, Cited1, Pdgfb, E2f8 and Mylk (Figure 2e).

Reportedly, Hmox1 (gene ID: 15368) is located in the cell nucleus, and has been proved to be involved in MSCs differentiation and to respond to 3D structure activation [21]. Notch4 (gene ID: 18132) is located in cytoplasmic vesicles and endoplasmic reticulum, and enables Notch binding activities that widely participate in directing cell fates or regulate the branching morphogenesis and homeostasis of multiple tissues and organs [29]. Cited1 (gene ID: 12705) is located in the cytosol and nucleus, and participates in embryonic placenta development, melanocyte differentiation, vasculogenesis and estradiol-dependent leptin actions [30]. Pdgfb (gene ID: 18591) is one of the well-known growth factors, and is involved in platelet-derived growth factor binding activity, receptor ligand activity, nervous system development and regulation of cell migration [31]. E2f8 (gene ID: 108961) is located in the cell nucleus, and participates in the regulation of hepatocytes [32] and anti-tumor CD4$^+$ T helper cells [33]. Mylk (gene ID: 107589) is located in cell–cell junctions, and is involved in the cellular response to calcium ions, potassium ions or xenobiotic stimulus, and participates in tonic smooth muscle contractions [34] and carcinoma progression [35].

Figure 2. Notch4 is one of the niche-dual-responding genes and is related to MSC stemness in the 3D matrix *in vitro*. Pairwise comparisons of (**a**) '3D MSC *vs* 2D MSC', (**b**) '3D iSG *vs* 2D MSC' and (**c**) '3D iSG *vs* 3D MSC' revealed differentially expressed genes. (**d**) GO analysis showed these differentially expressed genes were enriched in cell stemness- (green font) and angiogenesis- (yellow font) related GO terms. Overlapping filtered out 76 genes and the heat map shows their transcriptional profiles. The dotted box indicates a cluster of structural cue-responsive genes. (**e**) The intersection of these 76 genes with 'GO:0035239 tube morphogenesis'-enriched genes resulted in six candidate genes, i.e. Hmox1, Notch4, Cited1, Pdgfb, E2f8 and Mylk. *GO* Gene Ontology, *iSG* induced sweat gland, *MAPK* mitogen-activated protein kinase, *MSCs* mesenchymal stem cells

Notably, Notch signaling is an evolutionarily conserved cell communicating pathway and includes four transmembrane surface receptors (Notch1, 2, 3, 4), which have close crosstalk with EDA/EDAR/NF-κB [36], Wnt/ß-catenin/Lef1 [37], the Sonic Hedgehog [38] and the bone morphogenetic protein [39] signaling pathways that are proven to regulate SG developmental processes according to the literature. Very recently, we reported a correlational phenomenon between the spatiotemporal down-regulation of Notch1 along with mouse embryonic SGs *in vivo* and 2D-cultured mouse MSCs-committing to SG fates *in vitro* [20]. However, the roles of the Notch signaling pathway during mouse SG morphogenesis *in vivo*, especially in response to SG lineage-restricted niches with 3D architecture *in vitro*, remain largely unexplored. Hence, we next attempted to explore the role of Notch4 (gene ID: 18132) in mediating MSC differentiation in 3D-printed matrix and eccrine SG morphogenesis.

DAPT inhibits Notch4 significantly, but VPA only activates Notch4 mildly *in vitro*

The Notch signaling pathway was tuned by using VPA and DAPT, respectively. As DAPT powder was dissolved in DMSO, which exhibits potential cytotoxicity caused by corrosive injuries, we added an equal volume of DMSO into the cell medium (i.e. '2D DMSO' group) as a control group. Despite limited cell apoptosis at day 1 (indicated by arrows, supplementary Figure 1, see online supplementary material), cell densities of '2D DMSO' are similar to '2D MSC' and '2D VPA' groups at day 4, which indicates that DMSO exhibits negligible damage to cell proliferation. Comparatively, a decreased cell density was observed in the '2D DAPT' group at days 1 and 4 (indicated by arrows, Figure 3a), which suggested that inhibiting Notch signaling slowed down the proliferation rate of MSCs.

Immunofluorescence staining showed that Notch4 was inhibited after DAPT administration in both the 2D (Figure 3b, '2D DAPT' group) and 3D (Figure 3c, '3D DAPT' group) culture systems, but VPA only activates Notch4 to a limited extent (Figure 3b, '2D VPA' group) at day 4. Similarly, western blotting showed that Notch4 protein expression levels were significantly inhibited by DAPT and were mildly activated by VPA (Figure 3d) at day 4. The repeated Western blotting images were provided in Supplementary Figure 2 (see online supplementary material). Relative density quantification showed that DAPT significantly down-regulated Notch4 protein expression compared with the DMSO group (Figure 3e, $p = 0.007$) or VPA group (Figure 3e, $p = 0.01$) in the 2D culture system, and other groups (Figure 3e, $p < 0.01$) in the 3D culture system. No significant difference of Notch4 protein expression was detected between the MSC group and VPA group in the 2D culture system (Figure 3e).

In the terms of gene expression detected by RT-qPCR, despite that VPA moderately up-regulated Notch4 gene expression in the 2D culture system (Figure 3f, $p < 0.01$), Notch4 gene expression of the 2D VPA group was still lower than that of the 2D MSC group (green dotted line, Figure 3f).

In the 3D culture system, DAPT administration significantly down-regulated Notch4 gene expression compared with any other groups (Figure 3g, $p < 0.005$). No significance of Notch4 gene expression was detected between '3D MSC' and '3D DMSO' groups (Figure 3g), which indicated that pure DMSO negligibly affected Notch4 gene expression levels. Notably, Notch4 gene expression in the 3D culture system (i.e. 3D MSC group and 3D DMSO group) is universally higher than in the 2D culture system (green dotted line, Figure 3g). In addition, when DAPT was subsequently added after VPA (i.e. 'VPA + DAPT' group), both the notch4 protein levels (Figure 3d and e) and notch4 gene levels (Figure 3f) were only minorly down-regulated, which indicates that the initially administrated activator or inhibitor determines the tuning trends of Notch4 signals.

Taken together, both protein and gene levels of Notch4 are correspondingly tuned in response to the administration of DAPT or VPA. However, DAPT inhibits Notch4 significantly, but VPA only activates Notch4 to a limited extent *in vitro*.

Notch4 specifically regulates Oct4-related stemness of MSCs in 3D matrix *in vitro*

In the 2D cultured system, immunofluorescence staining showed that Oct4, a cell stemness marker, greatly decreased in the '2D DAPT' group and was minorly up-regulated in the '2D VPA' groups (Figure 3b). Similar to the trends of Notch4 expression, western blotting showed that Oct4 protein expression levels were significantly inhibited by DAPT and were mildly activated by VPA (Figure 3d) at day 4. Relative density quantifications showed that DAPT significantly down-regulated Oct4 protein expression compared with the DMSO group (Figure 3e, $p = 0.005$) or VPA group (Figure 3e, $p = 0.03$) in the 2D culture system, and other groups (Figure 3e, $p < 0.005$) in the 3D culture system. No significant difference of Oct4 protein expression was detected between MSC and VPA groups in the 2D culture system (Figure 3e).

In terms of gene expression detected by RT-qPCR, VPA only moderately up-regulated Oct4 gene expression in the 2D culture system (Figure 3f, $p < 0.05$), which indicates that the stemness of 2D-cultured MSCs inevitably decreased regardless of inhibiting or activating Notch signaling pathways. Intriguingly, both Notch4 and Oct4 gene expressions in '3D MSC' and '3D DMSO' groups are higher than in the '2D MSC' group (green dotted line, Figure 3g). Pure DMSO negligibly affected Oct4 gene expression level because no significance of Oct4 gene expression was detected between 3D MSC and 3D DMSO groups (Figure 3g). Upon inhibiting Notch signaling pathways in the '3D DAPT' group, both Notch4 ($p < 0.005$) and Oct4 ($p < 0.05$) gene expression were significantly down-regulated (Figure 3g). Taken together, both Notch4 and Oct4 expression is higher in 3D than 2D culture systems and Oct4 exhibits a similar profile to Notch4 in response to the administration of DAPT or VPA.

As DAPT and VPA non-selectively regulate all Notch receptors, we further detected the gene expression of Notch1,
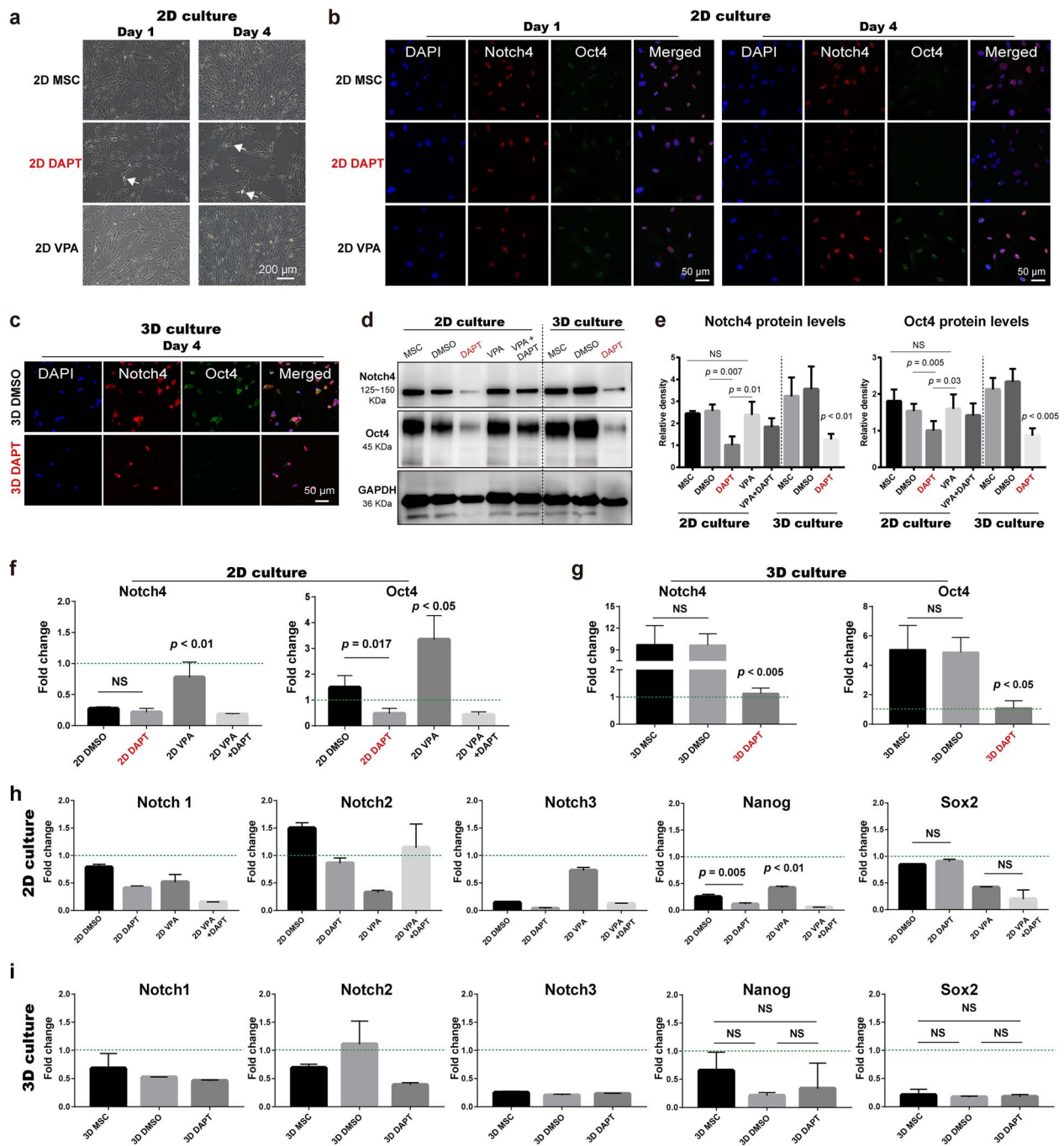
Figure 3. Notch4 specifically regulated Oct4-related stemness of MSCs in 3D matrix *in vitro*. (**a**) Inhibiting Notch signaling slowed down the proliferation rate of MSCs. Immunofluorescence staining of Notch4 and Oct4 in 2D culture system (**b**) and 3D culture system (**c**). (**d**) Western blotting images of Notch4 and Oct4 in response to administration of DAPT or VPA. (**e**) Relative density quantifications of Notch4 and Oct4 protein levels; n = 3. Gene expression of Notch4 and Oct4 exhibit a similar profile in both 2D culture system (**f**) (n = 3) and 3D culture system (**g**) (n = 3). Gene expressions of Notch1, 2, 3 and cell stemness markers (Nanog and Sox2) in 2D culture system (**h**) (n = 3) and 3D culture system (**i**) (n = 3). Green dotted lines indicate gene expression levels of '2D MSC' group (f–i). Scale bar (a): 200 μm; (b, c): 50 μm. *DAPT N*-[*N*-(3,5-Difluorophenacetyl-L-alanyl)]-(S)-phenylglycine *t*-butyl, *DMSO* dimethyl sulfoxide, *KDa* kilodalton, *MSCs* mesenchymal stem cells, *NS* no significant difference, *RT-qPCR* real-time quantitative polymerase chain reaction, *VPA* valproic acid

Notch2 and Notch3 in 2D and 3D culture systems by RT-qPCR. Notably, the gene expression of Notch1, Notch2 and Notch3 upon administration of DAPT and VPA were generally lower than in the '2D MSC' group both in 2D (green dotted line, Figure 3h) and 3D (green dotted line, Figure 3i) culture systems.

Furthermore, to explore the expression of other cell stemness markers, the gene expression of Nanog and Sox2 in 2D and 3D culture systems were also detected by RT-qPCR. Although Nanog gene expression in the '2D VPA' group is slightly up-regulated ($p < 0.01$, Figure 3h) in the 2D culture system, both Nanog and Sox2 were negligibly changed in

response to the administration of DAPT or VPA and their expression was generally lower than in the '2D MSC' group both in 2D (green dotted line, Figure 3h) and 3D (green dotted line, Figure 3i) culture systems.

Notch4 mediates SG differentiation of MSCs in the 3D model *in vitro*

To explore whether up-regulating Notch4 in the 2D culture system or down-regulating Notch4 in the 3D culture system could enhance SG differentiation of MSCs, VPA and DAPT were respectively administrated to PD-containing medium for inducing MSCs to differentiate into iSGs. PBS and DMSO were respectively employed as control groups. The expression of Notch4 and Krt18 was detected using immunofluorescence staining, western blotting and RT-qPCR, respectively. The gene expression of Krt14 and ATP1a1 as another two biomarkers of iSGs were also detected by RT-qPCR.

In the 2D culture system, administrating VPA only negligibly promoted Notch4 expression as determined by immunofluorescence staining (Figure 4a), Western blotting (PBS bands *vs* VPA bands in Figure 4c) and RT-qPCR (Figure 4d), which is consistent with results in Figure 3 that Notch4 expression exhibited a decreasing profile in the 2D culture system. In the 3D culture system, Notch4 expression was higher than in the 2D culture system as determined by immunofluorescence staining (PBS group in Figure 4a *vs* DMSO group in Figure 4b), western blotting (PBS bands *vs* DMSO bands in Figure 4c) and the RT-qPCR (PBS group *vs* DMSO group in Figure 4d), which is consistent with results in Figure 2d and RNA sequencing data that Notch4 belongs to a cluster of structural cue-responsive genes that were activated by the 3D culture environment. Upon administrating DAPT, Notch4 protein expression correspondingly decreased as determined by immunofluorescence staining (Figure 4b), western blotting (Figure 4c) and RT-qPCR ($p < 0.001$, Figure 4d).

In the 2D culture system, Krt18 immunofluorescence staining was weak in the PBS group and was only negligibly increased after administrating VPA (Figure 4a), and Krt18 protein levels of both the PBS and VPA groups in the 2D culture system are lower than in the 3D culture system as shown by western blotting (Figure 4c). Similar outcomes were found by RT-qPCR, i.e. both the SG phototype markers (Krt18 in Figure 4e, and Krt14 in Figure 4f) and the bio-functional marker (ATP1a1 in Figure 4g) in the 2D culture system are uniformly lower than in the 3D culture system.

In the 3D culture system, Krt18 immunofluorescence staining was strong in the DMSO group and DAPT administration subsequently reduced Krt18 expression (Figure 4b). Western blotting (Figure 4c) also showed that the Krt18 bands of the DMSO group are darker than in the DAPT group at days 1, 3 and 7. Similarly, the gene expression of Krt18 ($p = 0.003$, Figure 4e) and Krt14 ($p = 0.021$, Figure 4f) is significantly down-regulated upon DAPT administration at day 7. Despite there being no significant difference at day 7,

the ATP1a1 gene expression was significantly down-regulated upon DAPT administration at day 3 ($p = 0.026$, Figure 4g).

Notch signals regulate SG-originated cell stemness and are implicated in embryonic SG morphogenesis *in vivo*

As *in vitro* studies revealed that Notch4 participates in regulating Oct4-related cell stemness during MSCs commitment to SG lineages, we then asked whether Notch4 also participates in regulating the embryonic cell stemness or even affecting SG morphogenesis *in vivo*. To verify that, DAPT solutions were intraperitoneally injected into parent mice, and then immunohistochemistry staining of Notch4, Oct4 and Krt19 and immunofluorescence double-staining of Notch4 and K14 were performed in the next generation of mice at crucial time points (i.e. E12.5, E17.5, P1, P5 and P14) during SG development (Figure 5a).

For the control group, Notch4 was strongly expressed throughout skin tissues (i.e. epidermis, dermis, subcutaneous tissues) as well as other tissues (i.e. blood vessels, bones, muscles, etc.) at E12.5. Once SG buds emerged at E17.5, Notch4 intriguingly tended to be intensively expressed in skin tissues. Along with the process of SG morphogenesis, the overall distribution of Notch4 continuously decreased and was then restricted in epidermis, especially in the basal layers where SG buds emerged at P1. Notch4 almost disappeared in the newly formed glandular structures at P5 and in the mature SG at P14. For the DAPT group, Notch4 expression at E12.5 and E17.5 is distinctly reduced compared with control groups, especially in the basal layers of epidermis (Notch4 expression is indicated by red arrows, Figure 5b). Notably, Notch4-positive cells nearly disappeared in DAPT groups at P1, while Notch4 was still restrictedly expressed in the epidermis in control groups at P1. Taken together, Notch4 continuously decreased along with the process of SG morphogenesis in both control and DAPT groups, but injecting DAPT reduced Notch4 expression especially in embryonic periods (i.e. E12.5 and E17.5). Hence, we concluded that injecting parent mice with DAPT solutions down-regulated Notch4 expression in the next generation of mice, especially in the basal layers of the epidermis.

Similar to the decreasing profile of Notch4, the expression of both Oct4 and Krt19 was down-regulated in the DAPT group compared with the control group. Notably, Oct4-positive dermal stem cells distinctly decreased at P1 and P5 (Figure 5c), and K19-positive epidermal stem cells distinctly decreased in basal layers at E17.5, P1 and P5 (Figure 5d) in the DAPT group, which indicated that inhibiting the Notch signaling pathway using DAPT decreased the stemness of SG-originated cells at critical time points of SG morphogenesis.

To further verify whether the process of SG morphogenesis was delayed due to the reduced stemness of SG-originated cells, immunofluorescence co-staining of Notch4 and Krt14 was performed for monitoring the process of SG morphogenesis (Figure 5e). At E12.5, only a relatively small number of Krt14-positive SG progenitor cells were detected in both
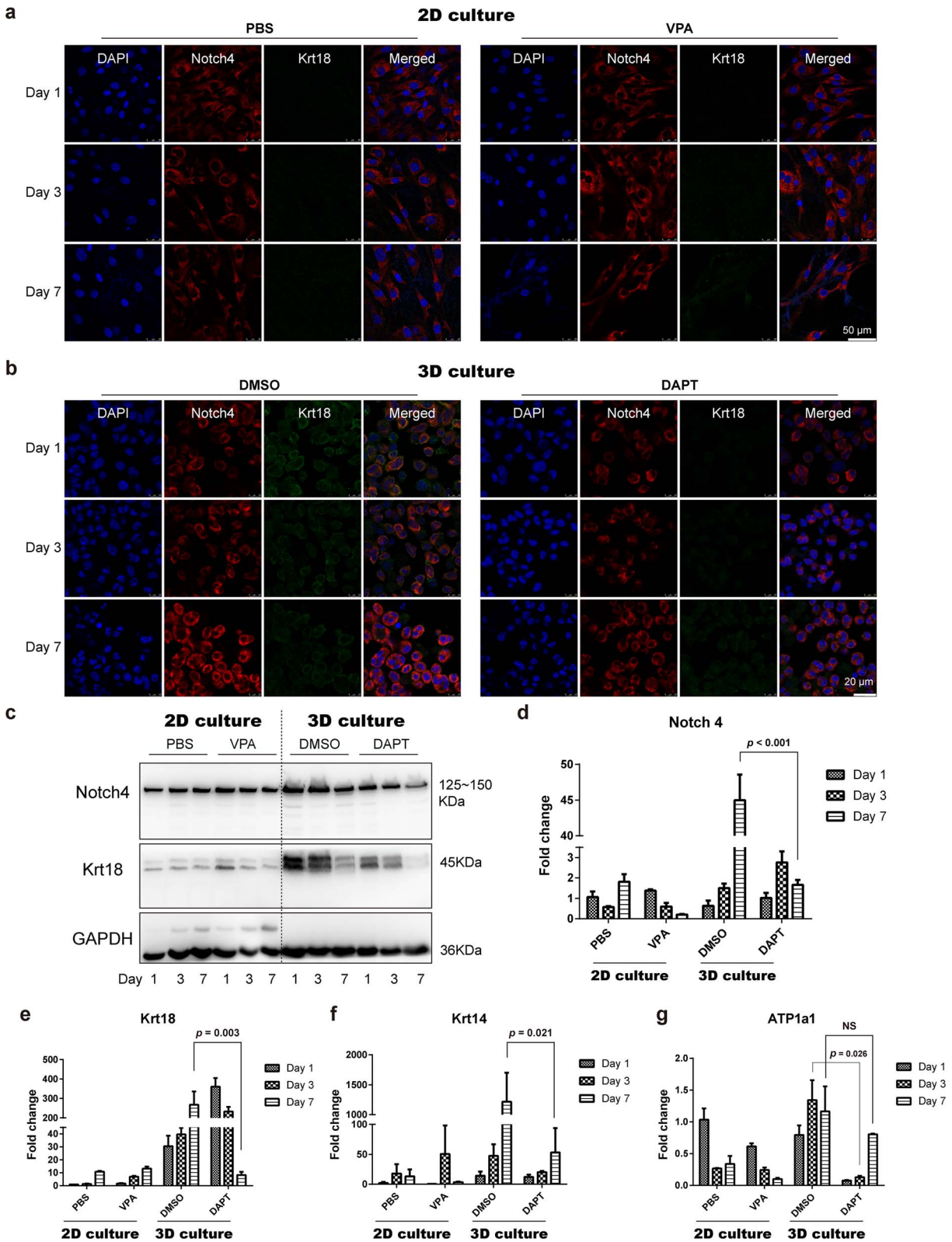
Figure 4. Notch4 mediates SG differentiation of MSCs in the 3D model *in vitro*. Immunofluorescence staining of Notch4 (red color) and Krt18 (green color) in 2D (**a**) and 3D (**b**) culture system. Western blotting of Notch4 and Krt18 in 2D and 3D culture system (**c**). Gene expression of Notch4 (**d**), Krt18 (**e**), Krt14 (**f**) and ATP1a1 (**g**); n = 3. Scale bar (a): 50 μm; (b): 20 μm. *ATP1a1* ATPase Na+/K+ transporting subunit alpha 1, *DAPT N*-[*N*-(3,5-difluorophenacetyl-L-alanyl)]-(S)-phenylglycine *t*-butyl, *DMSO* dimethyl sulfoxide, *KDa* kilodalton, *Krt* keratin, *MSCs* mesenchymal stem cells, *NS* no significant difference, *PBS* phosphate-buffered saline, *RT-qPCR* real-time quantitative polymerase chain reaction, *VPA* valproic acid
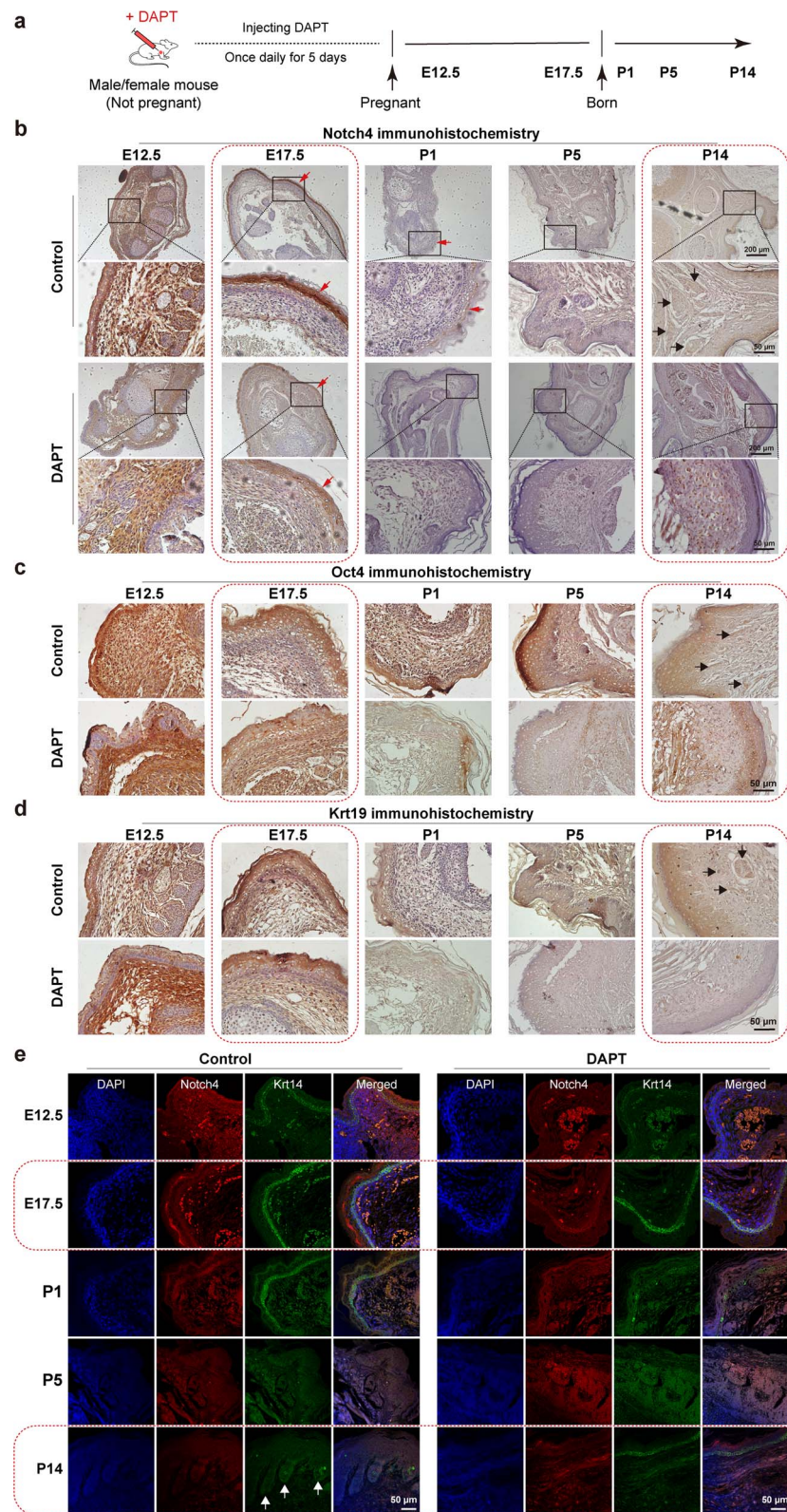
Figure 5. Notch signals regulate SG-originated cell stemness and are implicated in embryonic SG morphogenesis *in vivo*. Schematic drawings of DAPT injection and checking points, i.e. E12.5, E17.5, P1, P5 and P14 (**a**). Immunohistochemistry staining of Notch4 (**b**), Oct4 (**c**) and Krt19 (**d**). Immunofluorescence staining of Notch4 and Krt14 (**e**). Red arrows (b): Notch4-expressing positions. Black arrows (b–d) and white arrows (e): secretory coils of SG. Red dotted box (b–e): two critical time points during SG morphogenesis (i.e. E17.5 and P14). Scale bar (b): 200 μm, 50 μm; (c–e): 50 μm. *DAPT* N-[N-(3,5-Difluorophenacetyl-L-alanyl)]-(S)-phenylglycine *t*-butyl, *E* embryonic day, *Krt* keratin, *P* postpartum day, *SG* sweat gland

control and DAPT groups, possibly because SG morphogenesis has not begun. Even then, a slightly higher expression of Krt14 in the basal layer of the control group than the DAPT group is defined at E12.5. At E17.5 and P1, Krt14 expression was intensively concentrated in the basal layer of the epidermis, and more Krt14-positive SG progenitor cells were observed in the control group than in the DAPT group. Notably, compared with the control group, delayed SG morphogenesis with thinner gland ducts and shrunken glandular structures at both P5 and P14 were detected in the DAPT group (SGs are indicated by black arrows in Figure 5b–d and white arrows in Figure 5e, respectively).

Notch4 specifically targets epidermal stem cells and SG progenitor cells *in vivo*

Due to the non-selective inhibition of DAPT, anti-Notch4 monoclonal antibodies were intraperitoneally injected into pregnant mice in order to specifically inhibit Notch4 receptor without disturbing other Notch signaling-related molecules, and then SG morphogenesis was monitored at two critical time points (i.e. E17.5 and P14, Figure 6a).

Compared with the DAPT injection group (Figure 5b), injecting Notch4 monoclonal antibodies caused greater down-regulation of Notch4 expression (Figure 6b and e) followed by subsequently reduced expression of Krt19 (Figure 6d) and Krt14 (Figure 6e), which resulted in a more evident delay in SG morphogenesis with thinner gland ducts and shrunken glandular structures at E17.5 and P14. Comparatively, Krt14-positive cells were almost missing in the Notch4 antibody injection group at E17.5 (Figure 6e) but intensively concentrated Krt14 expression still remained in the basal layer of epidermis of the DAPT injection group at E17.5 (Figure 5e). However, Oct4 expression was negligibly changed in the Notch4 monoclonal antibodies injection group (Figure 6c) compare with the DAPT injection group (Figure 5c).

Discussion

The 3D-printed matrix exhibited satisfactory biodegradability, suitable inner microstructures, negligible cell deaths and multiple cell proliferations, which indicated the appropriate repeatability of 3D bioprinting approaches as well as good cell biocompatibility of 3D culture conditions. Notably, no significant difference in Krt18 gene expression in the '3D iSG' group was detected between day 1 and day 7, which could indicate that Krt18 was an early-stage biomarker and achieved high expression early with relatively high background expression levels during MSCs commitment to SG lineages. Taken together, MSCs committed to SG lineages in the artificial SG lineage-restricted niche *in vitro*.

Actually, 3D architectures represent the real scenarios in human tissues from the cells' own perspectives. Despite recent progress of multifarious bioactive materials in regenerative medicine [40], the chemical cues (i.e. drug-oriented small molecule compounds [41,42], protein factors [43], extracellular vesicles [44], etc.) seem to be overemphasized compared with structural cues in current stem cell-based therapies. The altered gene expression profiles aroused by pure structural cues have rarely been explored. Considering that '3D MSC *vs* 2D MSC' exhibited greater changes in genetic expression profile than '3D MSC *vs* 3D iSG', we speculate that structural cues have aroused greater transcriptional changes than biochemical cues during MSCs commitment to SG lineages. Interestingly, pure 3D-cultured MSCs still differentially expressed SG function-related biomarkers (i.e. ATP1a1 and Aqp5 genes) compared with 2D-cultured MSCs at day 7. Considering that no significant expression differences of SG phenotype-related biomarkers (i.e. Krt18 and Krt14 genes) were detected, we speculate that although pure 3D architecture can arouse transcriptional changes even without any chemical stimulation, pure structural cues are unable to direct MSCs towards SG lineages.

Among the six candidate genes, i.e. Hmox1, Notch4, Cited1, Pdgfb, E2f8 and Mylk, Notch4 mostly attracted our attention for the following reasons. (1) Notch4 belongs to a cluster of structural cue-responsive genes (marked by dotted box) whose expression levels are comparatively low in '2D MSC' groups but are higher in '3D MSC' and '3D iSG' groups (i.e. 3D-culture-endowed structural cues activated Notch4 expression). (2) Notch4 is proved to maintain the stemness of cancer stem cells [45], which implies that Notch4 possibly mediates SG differentiation by regulating MSC stemness *in vitro*. (3) Notch4 is involved in angiogenesis especially endothelial sprouting [46], which implies that Notch4 is possibly implicated in SG morphogenesis *in vivo* because capillary vasculatures reciprocally interact with SG lineage-restricted niches [47]. (4) Notch4 also regulates embryonic lymphangiogenesis [48] as well as the morphogenesis or carcinogenesis of other excretory glands, such as mammary glands [49] and salivary glands [50]. (5) Notch4 dually responded to both biochemical and structural cues and thus exhibited increased potential for exploitation in clinical use, especially considering that tuning of Notch signals showed potential for human tumor angiogenesis and obtained approval from the United States Food and Drug Administration [51]. Taken together, Notch4 serves as a promising niche-dual-responding gene that mediates SG lineages, and tuning Notch signals is likely to enter the clinic.

Notably, the cell stemness-related GO terms were enriched for '3D MSC *vs* 2D MSC' and '3D iSG *vs* 2D MSC' (green font) rather than '3D iSG *vs* 3D MSC'. In other words, 3D cultured cells up-regulated stemness-related genes compared with 2D cultured cells, but negligible changes of stemness-related genes were detected between the two groups of 3D-cultured cells even after MSCs had switched fate to SGs (i.e. 3D iSG *vs* 3D MSC). Additionally, the higher Oct4 expression verified that cell stemness was indeed elevated and maintained in 3D architectures. It could be illustrated that, compared with 2D-cultured cells, the elevated
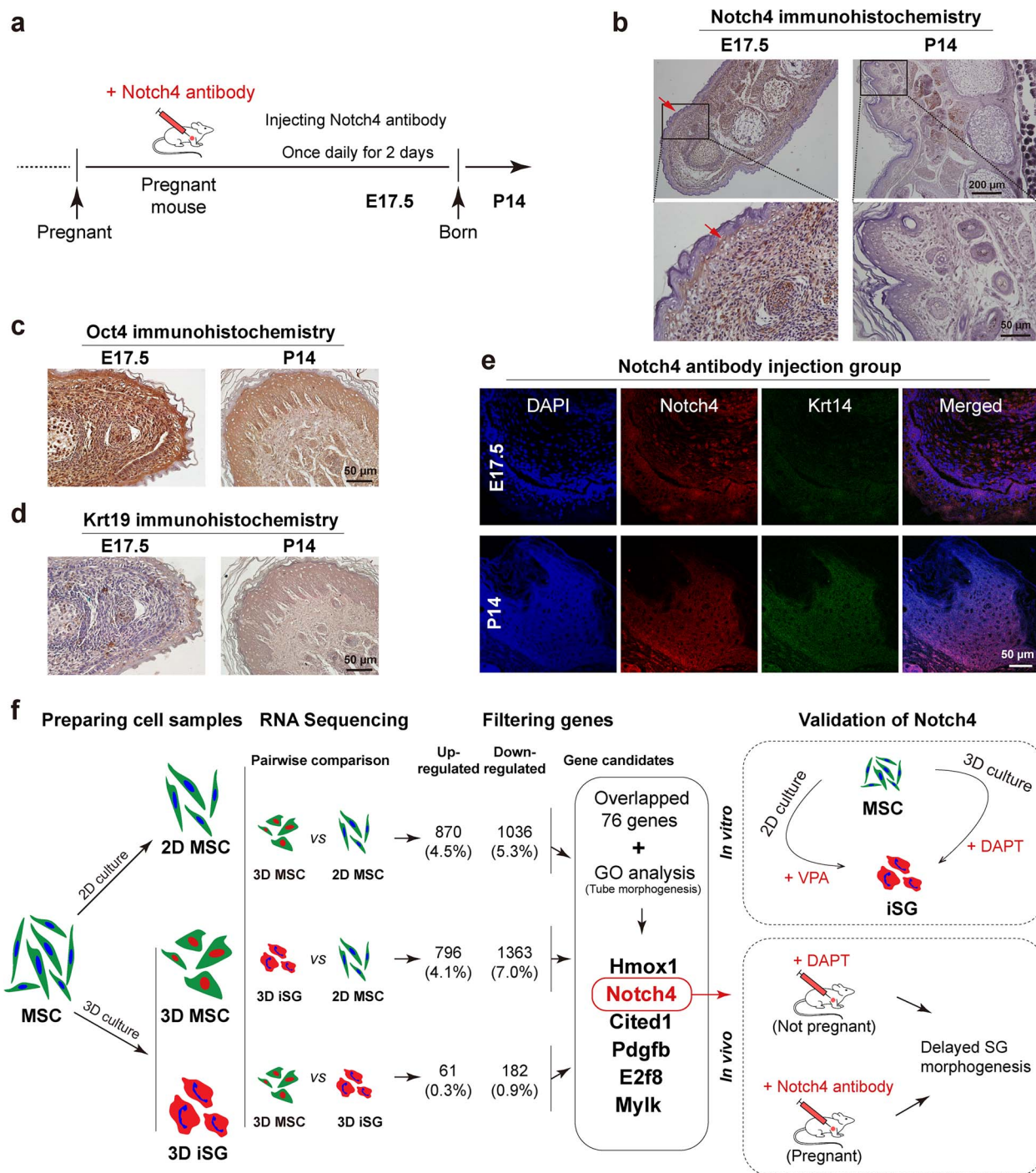
Figure 6. Notch4 specifically targets Krt19-positive epidermal stem cells and Krt14-positive SG progenitor cells *in vivo*. Schematic drawings of anti-Notch4 monoclonal antibodies injection and checking points, i.e. E17.5 and P14 (**a**). Immunohistochemistry staining of Notch4 (**b**), Oct4 (**c**) and Krt19 (**d**). Immunofluorescence staining of Notch4 (red color) and Krt14 (green color) (**e**). Flow chart of this study (**f**). Red arrows (b): Notch4-expressing positions. Scale bar (b): 200 μm, 50 μm; (e): 50 μm. *DAPT N-*[*N*-(3,5-Difluorophenacetyl-L-alanyl)]-(S)-phenylglycine *t*-butyl, *E* embryonic day, *GO* Gene Ontology, *iSG* induced sweat gland, *Krt* keratin, *MSCs* mesenchymal stem cells, *P* postpartum day, *SG* sweat gland, *VPA* valproic acid

stemness endows 3D cultured cells with enhanced abilities of proliferation and immigration so as to spread and immigrate throughout the 3D matrix. Intriguingly, not only were Notch4 and Oct4 both up-regulated in the 3D culture system but they also exhibited similar profiles in response to the administration of DAPT or VPA. Moreover, only Notch4

was differentially expressed compared with other Notch receptors (i.e. Notch1, 2, 3), and only Oct4 was activated compared with other cell stemness markers (i.e. Nanog and Sox2), which implies that Notch4 specifically targets Oct4-related MSC stemness, and 3D architecture only promotes limited cell stemness *in vitro*.

To validate the role of Notch4 in SG differentiation *in vitro*, VPA and DAPT were respectively added to the PD-containing medium for inducing MSCs to differentiate into iSGs. Based on the background expression levels of Notch4, Notch signals were up-regulated in the 2D culture system and were down-regulated in the 3D culture system. Notably, in the 2D culture system, fate-switching from MSCs to iSGs still failed even if Notch signals were activated, which indicated that both biochemical and structural cues are indispensable for SG differentiation. In the 3D culture system, inhibiting Notch signals prevented SG differentiation, indicating that Notch signals participate in SG differentiation of MSCs *in vitro*.

To further validate the role of Notch4 in embryonic SG morphogenesis *in vivo*, DAPT and anti-Notch4 monoclonal antibodies were respectively injected into mice, thus further delaying embryonic SG morphogenesis. Notably, DAPT non-selectively inhibited the expression of Oct4, Krt19 and Krt14, while anti-Notch4 monoclonal antibodies negligibly affect Oct4 expression, but selectively target Krt19 and Krt14 expression, which indicates that Notch4 specifically targets Krt19-positive epidermal stem cells and Krt14-positive SG progenitor cells that are closely involved in mouse SG morphogenesis *in vivo*.

Conclusions

MSCs committed to SG lineages in the artificial SG lineage-restricted niche based on the synergistic interactions of structure and biochemical cues. Notch4 acts as an SG niche-dual-responding gene, which not only mediates SG differentiation by affecting MSC stemness in artificial SG lineage-restricted niches *in vitro* but is also implicated in SG embryonic morphogenesis by specifically targeting Krt19-positive epidermal stem cells and Krt14-positive SG progenitor cells *in vivo*. Tuning Notch4 signal represents a promising molecular target for stem cell-based SG regenerative therapies.

Acknowledgments

We are grateful for the kind assistance of all the members in our lab.

Abbreviations

ATP1a1: ATPase Na+/K+ transporting subunit alpha 1; Aqp5: Aquaporin 5; DAPT: *N*-[*N*-(3,5-Difluorophenacetyl-L-alanyl)]-(*S*)-phenylglycine *t*-butyl; DMSO: Dimethyl sulfoxide; E: embryonic day; GO: Gene ontology; iSG: Induced sweat gland; KDa: Kilodalton; Krt: Keratin; MAPK: Mitogen-activated protein kinase; MSCs: Mesenchymal stem cells; NS: No significant difference; P: Postpartum day; PBS: Phosphate-buffered saline; PD: Plantar dermis; RT-qPCR: Real-time quantitative polymerase chain reaction; SG: Sweat gland; VPA: Valproic acid.

Supplementary data

Supplementary material is available at *Burns & Trauma Journal* online.

Authors' contributions

YZW: conception and design, financial support, collection of data, data analysis and interpretation, and manuscript writing. FLZ and BY: administrative support, provision of study materials, and assembly of data. LHH: provision of study materials and assembly of data. ZL, WS, YK and YXT: administrative support and assembly of data. XBF and SH: financial support, provision of study materials and final approval of the manuscript.

Data availability

All the data and materials in this study are available from the corresponding author upon reasonable request.

Ethics approval and consent to participate

The Institutional Animal Care and USE Committee of Chinese PLA General Hospital (Beijing, China) approved the animal experiments (approval number SCXK(BJ)2019–0001) and supervised the animal welfares of this study.

Consent for publication

All authors have agreed to provide their consent for publication.

Conflict of interest

Any commercial or financial relationships that could be construed as a potential conflict of interest were absent of this research.

References

1. Lu CP, Polak L, Rocha AS, Pasolli HA, Chen SC, Sharma N, *et al*. Identification of stem cell populations in sweat glands and ducts reveals roles in homeostasis and wound repair. *Cell*. 2012;150:136–50.
2. C.P. Lu, L. Polak, B.E. Keyes, E. Fuchs, Spatiotemporal antagonism in mesenchymal-epithelial signaling in sweat versus hair fate decision, *Science* (New York, N.Y.). 2016;354:6319.
3. Lu C, Fuchs E. Sweat gland progenitors in development, homeostasis, and wound repair. *Cold Spring Harbor perspectives in medicine*. 2014;4:2.
4. Wang R, Wang Y, Yao B, Hu T, Li Z, Liu Y, *et al*. Redirecting differentiation of mammary progenitor cells by 3D bioprinted sweat gland microenvironment. *Burns Trauma*. 2019;7:29.
5. Chee MK, Jo SK, Sohn KC, Kim CD, Lee JH, Lee YH. Effects of Brn2 overexpression on eccrine sweat gland development in the mouse paw. *Biochem Biophys Res Commun*. 2017;490:901–5.

6. Xie J, Yao B, Han Y, Shang T, Gao D, Yang S, *et al*. Cytokeratin expression at different stages in sweat gland development of C57BL/6J mice. *Int J Low Extrem Wounds*. 2015;14:365–71.

7. Scadden DT. The stem-cell niche as an entity of action. *Nature*. 2006;441:1075–9.

8. Morrison SJ, Spradling AC. Stem cells and niches: mechanisms that promote stem cell maintenance throughout life. *Cell*. 2008;132:598–611.

9. Nabhan AN, Brownfield DG, Harbury PB, Krasnow MA, Desai TJ. Single-cell Wnt signaling niches maintain stemness of alveolar type 2 cells. *Science*. 2018;359:1118–23.

10. Vining KH, Mooney DJ. Mechanical forces direct stem cell behaviour in development and regeneration. *Nat Rev Mol Cell Biol*. 2017;18:728–42.

11. Scadden DT. Nice neighborhood: emerging concepts of the stem cell niche. *Cell*. 2014;157:41–50.

12. Pinho S, Frenette PS. Haematopoietic stem cell activity and interactions with the niche. *Nat Rev Mol Cell Biol*. 2019;20:303–20.

13. Lei M, Schumacher LJ, Lai YC, Juan WT, Yeh CY, Wu P, *et al*. Self-organization process in newborn skin organoid formation inspires strategy to restore hair regeneration of adult cells. *Proc Natl Acad Sci U S A*. 2017;114:E7101–e7110.

14. Hosseini M, Koehler KR, Shafiee A. Biofabrication of human skin with its appendages. *Advanced healthcare materials*. 2022;11:22, e2201626.

15. Sun X, Xiang J, Chen R, Geng Z, Wang L, Liu Y, *et al*. Sweat gland organoids originating from reprogrammed epidermal keratinocytes functionally recapitulated damaged skin. *Advanced science*(Weinheim, Baden-Wurttemberg, Germany). 2021;8:e2103079.

16. Fu NY, Nolan E, Lindeman GJ, Visvader JE. Stem cells and the differentiation hierarchy in mammary gland development. *Physiol Rev*. 2020;100:489–523.

17. Zhang Y, Enhejirigala B, Yao Z, Li W, Song JL, Li J, *et al*. Using bioprinting and spheroid culture to create a skin model with sweat glands and hair follicles, burns. *Trauma*. 2021;9: tkab013.

18. Liu Y, Li J, Yao B, Wang Y, Wang R, Yang S, *et al*. The stiffness of hydrogel-based bioink impacts mesenchymal stem cells differentiation toward sweat glands in 3D-bioprinted matrix, materials science & engineering. C, *Materials for biological applications*. 2021;118:111387.

19. Ferraris C, Chevalier G, Favier B, Jahoda CA, Dhouailly D. Adult corneal epithelium basal cells possess the capacity to activate epidermal, pilosebaceous and sweat gland genetic programs in response to embryonic dermal stimuli. *Development (Cambridge, England)*. 2000;127:5487–95.

20. Wang Y, Yao B, Duan X, Li J, Song W, Enhejirigala, *et al*. Notch1 down-regulation in lineage-restricted niches is involved in the development of mouse eccrine sweat glands. *J Mol Histol*. 2022;53:857–67.

21. Yao B, Wang R, Wang Y, Zhang Y, Hu T, Song W, *et al*. Biochemical and structural cues of 3D-printed matrix synergistically direct MSC differentiation for functional sweat gland regeneration. *Sci Adv*. 2020;6:eaaz1094.

22. Mohammed TA, Holen KD, Jaskula-Sztul R, Mulkerin D, Lubner SJ, Schelman WR, *et al*. A pilot phase II study of valproic acid for treatment of low-grade neuroendocrine carcinoma. *Oncologist*. 2011;16:835–43.

23. Tao ZS, Li TL, Xu HG, Yang M. Hydrogel contained valproic acid accelerates bone-defect repair via activating Notch signaling pathway in ovariectomized rats. *Journal of materials science Materials in medicine*. 2021;33:4.

24. Breuls N, Giarratana N, Yedigaryan L, Garrido GM, Carai P, Heymans S, *et al*. Valproic acid stimulates myogenesis in pluripotent stem cell-derived mesodermal progenitors in a NOTCH-dependent manner. *Cell Death Dis*. 2021;12: 677.

25. Hu N, Zhang X, Zhang X, Guan Y, He R, Xue E, *et al*. Inhibition of Notch activity suppresses hyperglycemia-augmented polarization of macrophages to the M1 phenotype and alleviates acute pancreatitis. *Clin Sci*(London, England: 1979). 2022;136:455–71.

26. Wei J, Zhang L, Ren L, Zhang J, Yu Y, Wang J, *et al*. Endosulfan inhibits proliferation through the Notch signaling pathway in human umbilical vein endothelial cells. *Environ Pollut*(Barking, Essex : 1987). 2017;221:26–36.

27. Cheng X, Yu Z, Xu J, Quan D, Long H. Pathophysiological changes and the role of Notch-1 activation after decompression in a compressive spinal cord injury rat model. *Front Neurosci*. 2021;15:579431.

28. Ahmed AA, Robinson T, Palande M, Escara-Wilke J, Dai J, Keller ET. Targeted Notch1 inhibition with a Notch1 antibody, OMP-A2G1, decreases tumor growth in two murine models of prostate cancer in association with differing patterns of DNA damage response gene expression. *J Cell Biochem*. 2019;120:16946–55.

29. Zhou B, Lin W, Long Y, Yang Y, Zhang H, Wu K, *et al*. Notch signaling pathway: architecture, disease, and therapeutics. *Signal transduction and targeted therapy*. 2022;7:95.

30. González-García I, García-Clavé E, Cebrian-Serrano A, Thuc Le, Contreras RE, Xu Y, *et al*. Estradiol regulates leptin sensitivity to control feeding via hypothalamic Cited1. *Cell Metab*. 2023;35:438–455.e7.

31. Chen Z, Soni N, Pinero G, Giotti B, Eddins DJ, Lindblad KE, *et al*. Monocyte depletion enhances neutrophil influx and proneural to mesenchymal transition in glioblastoma. *Nat Commun*. 2023;14:1839.

32. Jin Y, Anbarchian T, Wu P, Sarkar A, Fish M, Peng WC, *et al*. Wnt signaling regulates hepatocyte cell division by a transcriptional repressor cascade. *Proc Natl Acad Sci U S A*. 2022;119:e2203849119.

33. Park SA, Lim YJ, Ku WL, Zhang D, Cui K, Tang LY, *et al*. Opposing functions of circadian protein DBP and atypical E2F family E2F8 in anti-tumor Th9 cell differentiation. *Nat Commun*. 2022;13:6069.

34. Isselbacher EM, Lino Cardenas CL, Lindsay ME. Hereditary influence in thoracic aortic aneurysm and dissection. *Circulation*. 2016;133:2516–28.

35. Li J, Xu X, Liu C, Xi X, Wang Y, Wu X, *et al*. miR-181a-2-3p stimulates gastric cancer progression via targeting MYLK. *Frontiers in bioengineering and biotechnology*. 2021;9:687915.

36. Kamberov YG, Wang S, Tan J, Gerbault P, Wark A, Tan L, *et al*. Modeling recent human evolution in mice by expression of a selected EDAR variant. *Cell*. 2013;152:691–702.

37. Cluzeau C, Hadj-Rabia S, Jambou M, Mansour S, Guigue P, Masmoudi S, *et al*. Only four genes (EDA1, EDAR, EDARADD, and WNT10A) account for 90% of hypohidrotic/anhidrotic ectodermal dysplasia cases. *Hum Mutat*. 2011;32:70–2.

38. Cui CY, Kunisada M, Childress V, Michel M, Schlessinger D. Shh is required for Tabby hair follicle development. *Cell Cycle*(Georgetown, Tex.). 2011;10:3379–86.

39. Närhi K, Tummers M, Ahtiainen L, Itoh N, Thesleff I, Mikkola ML. Sostdc1 defines the size and number of skin appendage placodes. *Dev Biol*. 2012;364:149–61.

40. Wang Y, Yuan X, Yao B, Zhu S, Zhu P, Huang S. Tailoring bioinks of extrusion-based bioprinting for cutaneous wound healing. *Bioactive materials*. 2022;17:178–94.

41. Guo Y, Wang YY, Sun TT, Xu JJ, Yang P, Ma CY, *et al*. Neural progenitor cells derived from fibroblasts induced by small molecule compounds under hypoxia for treatment of Parkinson's disease in rats. *Neural Regen Res*. 2023;18: 1090–8.

42. Zhao A, Qin H, Sun M, Tang M, Mei J, Ma K, *et al*. Chemical conversion of human epidermal stem cells into intestinal goblet cells for modeling mucus-microbe interaction and therapy. *Sci Adv*. 2021;7:16.

43. Qin H, Zhao AD, Sun ML, Ma K, Fu XB. Direct conversion of human fibroblasts into dopaminergic neuron-like cells using small molecules and protein factors. *Mil Med Res*. 2020; 7:52.

44. Lang HL, Zhao YZ, Xiao RJ, Sun J, Chen Y, Hu GW, *et al*. Small extracellular vesicles secreted by induced pluripotent stem cell-derived mesenchymal stem cells improve postoperative cognitive dysfunction in mice with diabetes. *Neural Regen Res*. 2023;18:609–17.

45. Zhou L, Wang D, Sheng D, Xu J, Chen W, Qin Y, *et al*. NOTCH4 maintains quiescent mesenchymal-like breast cancer stem cells via transcriptionally activating SLUG and GAS1 in triple-negative breast cancer. *Theranostics*. 2020;10:2405–21.

46. MacKenzie F, Duriez P, Larrivée B, Chang L, Pollet I, Wong F, *et al*. Notch4-induced inhibition of endothelial sprouting requires the ankyrin repeats and involves signaling through RBP-Jkappa. *Blood*. 2004;104:1760–8.

47. Yuan X, Duan X, Enhejirigala Z, Li B, Yao WS, Song W, *et al*. Reciprocal interaction between vascular niche and sweat gland promotes sweat gland regeneration. *Bioactive materials*. 2023;21:340–57.

48. Muley A, Kim Uh M, Salazar-De Simone G, Swaminathan B, James JM, Murtomaki A, *et al*. Unique functions for Notch4 in murine embryonic lymphangiogenesis. *Angiogenesis*. 2022;25:205–24.

49. Bonadeo N, Becu-Villalobos D, Cristina C, Lacau-Mengido IM. The Notch system during pubertal development of the bovine mammary gland. *Sci Rep*. 2019;9:8899.

50. Ho AS, Ochoa A, Jayakumaran G, Zehir A, Valero Mayor C, Tepe J, *et al*. Genetic hallmarks of recurrent/metastatic adenoid cystic carcinoma. *J Clin Invest*. 2019;129:4276–89.

51. Cook KM, Figg WD. Angiogenesis inhibitors: current strategies and future prospects. *CA Cancer J Clin*. 2010;60:222–43.